Journal of Sedimentary Environments (2023) 8:545–561
https://doi.org/10.1007/s43217-023-00152-8

RESEARCH

Geochemistry of Kuldhar Member Limestone (Callovian–Oxfordian), Jaisalmer Basin, western Rajasthan, India: implications on depositional conditions and sources of rare earth elements

Shaikh Asjad[1] · Kr. Farahim Khan[1] · M. A. Quasim[1] · Aashna Javed[1]

Received: 25 July 2023 / Revised: 4 September 2023 / Accepted: 12 September 2023 / Published online: 10 October 2023

Abstract
The present study examines the distribution of major and rare earth elements (REEs) in the Kuldhar Member Limestone (KML), Jaisalmer Formation, western Rajasthan, India. The study aims to gain insight into the sources of REEs and the depositional environment using petrographical and geochemical studies. The dominant major oxide is CaO, primarily originating from biogenic sources due to the high fossil content of the member. The dominance of CaO implies that calcite was the primary mineral phase in these carbonates. Following CaO, iron oxide (Fe_2O_3) is the next abundant component. The higher concentration of Fe can be attributed to its adsorption onto clay components, explaining the strong correlation between Fe_2O_3 and Al_2O_3 ($r = 0.93$), as well as the excess Fe content. The relatively higher concentration of $\sum$REE in the samples indicate that there have been some detrital siliciclastic fractions. The Post Archaean Australian Shale (PAAS) normalized pattern is nearly flat, with variable Ce and Gd anomalies, as well as a positive Eu anomaly. The higher $(Nd/Yb)_{SN}$ ratio (avg. 1.20) indicates that these samples did not retain their original seawater properties, which is further supported by the extremely low Er/Nd ratio (avg. 0.09). The $(Dy/Yb)_{SN}$ ratio (avg. 1.42) is observed to be similar to shallow marine and Indian Ocean carbonate. A higher $(Dy/Yb)_{SN}$ ratio suggests that heavy rare earth elements (HREEs) are slightly more enriched than light rare earth elements (LREEs), which is similar to modern seawater. The variable Ce anomaly reflects changes in terrigenous input into the system. Notably, fluctuations in the Ce anomaly value and Mn* values are indicative of alternating oxic and anoxic depositional environmental conditions. These variations correspond to several short-term changes in global climatic conditions during the Middle Jurassic period.

Keywords Carbonate geochemistry · Depositional environment · REEs source · Callovian–Oxfordian · Jaisalmer Basin

1 Introduction

Depositional environments refer to specific areas, where sediments accumulate over a significant period, characterized by unique physical, chemical, and biological conditions (Reineck & Singh, 1980). The chemical composition of carbonate rocks can effectively indicate the environmental conditions prevalent during their deposition. Rare earth elements (REEs) typically have a +3 oxidation state, except 'Ce' and 'Eu', and exhibit similar ionic radii under most physico-chemical conditions in the Earth's crust. Analysing the distribution of REE concentrations in ancient carbonate rocks provides valuable insights into distinguishing between marine and non-marine sources of REEs (Banner et al., 1988; Frimmel, 2009). REEs have low solubility and tend to remain immobile during post-depositional processes, such as diagenesis and metamorphism (Muecke et al., 1979). REEs in sedimentary rocks are highly sensitive to changes in the depositional environment, making them a reliable tool for reconstructing palaeoenvironments (Wan et al., 2017). Previous studies have demonstrated that the concentration, partitioning behaviour, and elemental anomalies of REEs in carbonate rocks can serve as a proxy for interpreting the depositional environment and provide valuable insights into the processes involved in their formation (Lv et al., 2020). In addition, the analysis of REE concentrations in sedimentary rocks can shed light on various geological processes,

Communicated by M. V. Alves Martins

✉ Shaikh Asjad
shaikhasjad94@gmail.com

[1] Department of Geology, Aligarh Muslim University, Aligarh, UP 202002, India

including the evolution of the lithosphere over time, sediment deposition environments, tectonic activity, and magmatism (Bau & Dulski, 1996; Taylor & McLennan, 1985).

Numerous researchers have investigated the distribution of REEs in marine waters, sediments, and carbonate rocks (De Baar et al., 1988; Elderfield et al., 1990; Nagarajan et al., 2011; Patra & Singh, 2017; Singh et al., 2019; Webb & Kamber, 2000). Several factors, including terrestrial inputs through weathering and hydrothermal activity, scavenging processes, salinity, and oxygen levels, significantly influence the concentrations of REEs in seawater (Elderfield, 1988). In the case of carbonate rocks, the depositional environment plays a major role in shaping the observed patterns of REEs (Madhavaraju & Ramasamy, 1999; Murray et al., 1992). Other factors such as extensive oceanic redox conditions (Liu et al., 1988), variations in surface productivity (Toyoda et al., 1990), lithology and diagenesis (Fu et al., 2011; Nath et al., 1992), as well as paleogeography and depositional models (Kamber & Webb, 2001), also impact the distribution of REEs in carbonate rocks.

The Jaisalmer Basin boasts a remarkable preservation of Jurassic marine environmental changes, captivating geoscientists from various disciplines. This fascination arises from the abundance of well-preserved marine fossils, dinosaur footprints, condensed sequences, hardgrounds, soft-sediment deformation structures, shell beds, and extensive carbonate sedimentary sequences (Ahmad et al., 2017, 2020, 2021a; Asjad et al., 2021; Pandey & Pooniya, 2015). The present study focuses on interpreting advanced geochemical data of major and rare earth elements in the Callovian–Oxfordian Kuldhar Member Limestone (KML) to investigate the variations and distributions of these elements. The aim is also to utilise the REEs as potential proxies for understanding the palaeoenvironmental conditions during the deposition of these rocks, as previously done by Wan et al. (2017). To date, there has been a lack of comprehensive geochemical investigations and no utilization of an REE-based approach to interpret the depositional environment of the limestone of Kuldhar Member in the Jaisalmer Formation. Therefore, this research holds significant importance as it examines the relationship between REE concentrations and the depositional environment in the KML. These findings will also contribute to the reconstruction of the ancient marine environment and provide valuable insights into the sedimentary processes and conditions during that time, palaeoclimate, water chemistry, and other relevant aspects of the Jurassic period in the Jaisalmer Basin. Thus, this research represents a significant contribution with the potential to enhance our understanding of the Jurassic history of the Jaisalmer Basin and its geological significance.

2 Geological setting

The Jaisalmer Basin is located on the north-western slope of the Indian craton. It encompasses the entire Jaisalmer district in western Rajasthan, India (Fig. 1). It is classified as a pericratonic shelf basin. The formation of the Jaisalmer Basin was initiated during the Jurassic period by the breaking of the Indian plate from the southern continent. This was subsequently followed by sequential rifting and repetitive movements associated with the northward drift of the Indian plate. The Jaisalmer Basin covers ~ 45,000 Km^2 and has been classified as a category-I basin (onland) with commercial production, according to a report from the Directorate General of Hydrocarbons (DGH-2019–20). The Jaisalmer Basin has experienced fluctuations in sea levels caused by tectonic and climatic factors, resulting in periods of transgression and regression throughout its history. The basin became geologically active after the Mesozoic era and is categorized into four distinct structural units. These units include: (a) the elevated Mari-Jaisalmer arch, which extends in a northwest to southeast direction; (b) the Shahgarh sub-basin, a syncline trending southwest; (c) the Kishangarh sub-basin located to the north–northeast; and (d) the Miajlar sub-basin situated in the southern region.

In comparison with the neighbouring Kachchh Basin, the Jurassic sedimentary sequence in the Jaisalmer Basin is relatively thinner and represents distinct depositional environments (Ahmad et al., 2017, 2020, 2021a, 2021b, 2022; Pandey et al., 2009, 2010). Most Mesozoic rocks in the basin are covered by desert, with sporadically exposed sections. The lithostratigraphic division of the basin comprises the Lathi, Jaisalmer, Baisakhi, and Bhadasar Formations, each consisting of several additional members. During Mesozoic sedimentation, the Lathi Formation initially witnessed the deposition of fluvial, lacustrine, deltaic, and marginal marine sediments (Ahmad et al., 2020; Srivastava, 1966). Shallow marine deposits characterize the subsequent Jaisalmer, Baisakhi, and Bhadasar Formations. The Jaisalmer Formation, named by Swami Nath et al. (1959), was further classified into four lithostratigraphic members: Joyan, Fort, Badabag, and Kuldhar, as outlined by Narayanan et al. (1961). Das Gupta (1975) introduced the Hamira Member at the base, and later, Kachhara and Jodhawat (1981) added the Jajiya Member at the top, bringing the total number of members within the Jaisalmer Formation to six (Table 1).

2.1 Study area geology

The rocks of Kuldhar Member of the Jaisalmer Formation are poorly cemented and have limited exposure. The type

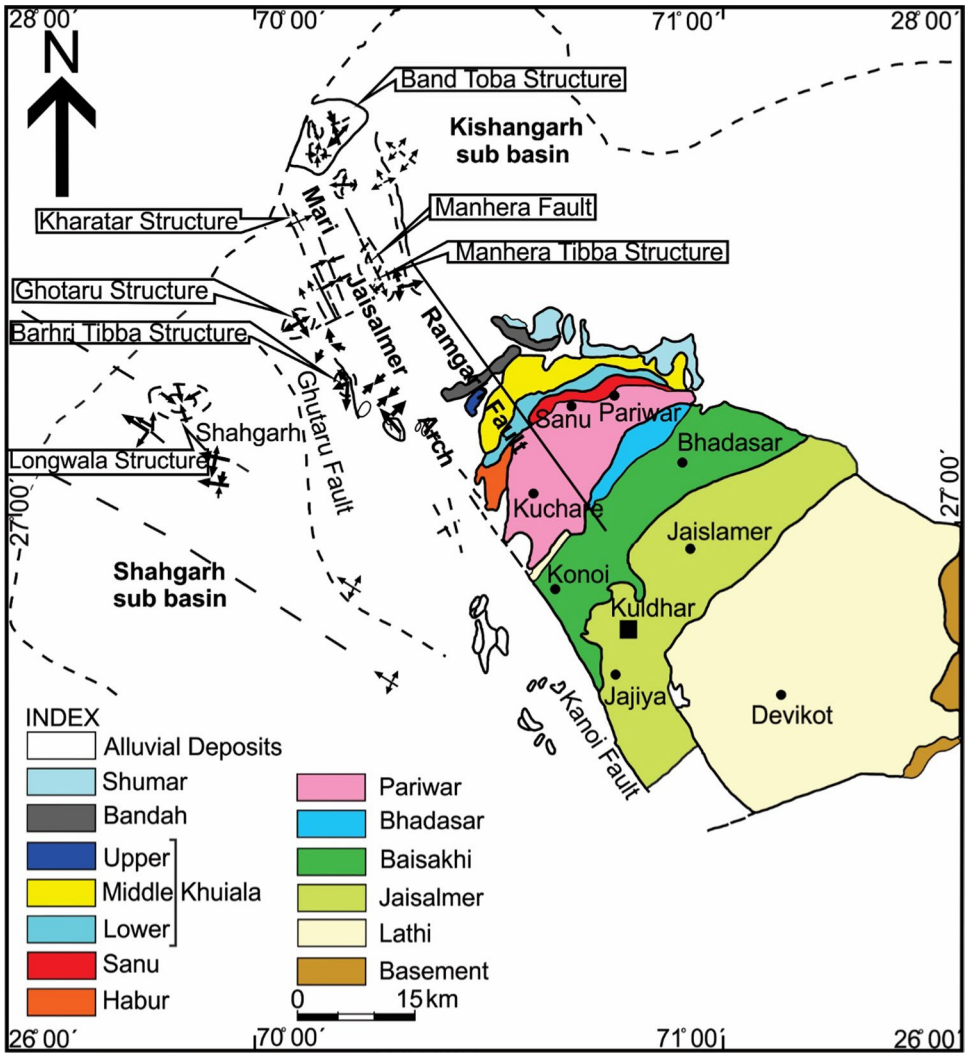

Fig. 1 Geological map of the Jaisalmer Basin (after Das Gupta, 1975)

area of Kuldhar Member is best exposed around the dry beds of Kuldhar River, southwest of the erstwhile Kuldhar village. Two sections were measured (Fig. 2a, b); the Kuldhar River Section starts with uppermost part of the Upper Bathonian Badabag Member, which is exposed as a platform and forms the basement for the Kuldhar sequences. The Badabag Member is exposed on the eastern side of the Kuldhar River just southwest of the abandoned Kuldhar village. Fine-grained sandstone marks the beginning of Badabag Member sediments, followed by limestone beds with mega ripples (Fig. 3a) and iron encrusted hardgrounds (Fig. 3b). The rocks of the Kuldhar Member with a thickness of approximately 7 m, consist of alternate beds of ferruginous shale (Fig. 3c) (Asjad et al., 2021) and poorly cemented limestone (Fig. 3c). The Kuldhar Nala Section, with a thickness of 2.5 m, consists of alternate shale and well-cemented limestone (Fig. 3d). This section comprises diverse fossil assemblages, including brachiopods, bivalves, belemnites and oysters (Fig. 3e). The presence of alternating bands of shale and limestone indicates fluctuating energy conditions and variations in depositional environments. The shale present here is Fe-shale (Asjad et al., 2021). Another hillock of gypsiferous shale (Fig. 3f) is located near the Kuldhar River, but as the gypsum is of secondary origin, it is not suitable for studies related to the depositional environment. The Kuldhar Member is the most fossiliferous unit of the Jaisalmer Formation, containing Callovian ammonites (such as *Macrocephalites semilaevis* and *Reineckeia (Reineckeia) anceps*, etc.), nautiloids, brachiopods, echinoderms, ostracods, gastropods, corals, algae and foraminifers (Jain, 2008; Pandey et al., 2010). The Kuldhar Member has been assigned a Callovian age based on the presence of Callovian ammonites.

Table 1 Lithostratigraphic scheme of the Jurassic strata of the Jaisalmer Basin (after Asjad et al., 2021; Pandey & Pooniya, 2015)

Formation	Member		Age	Lithology
Bhadasar	Mokal		? Lower cretaceous	Brown, well-cemented, argillaceous sandstone with wood fossils
	Kolar Dungar		Tithonian	Bands of ferruginous coarse-grained sandstones alternating with loosely cemented red sandstones
Baisakhi	Lanela	Ludharwa	Tithonian–Oxfordian	Intercalations of fine-grained, light brown argillaceous sandstone and grey shales with ammonites. Gypseous clay bands with poorly developed current-beddings at the top of this member
	Rupsi			Brown, hard, argillaceous sandstone with intraformational conglomerate
	Basal			Grey to black shale, very often ferruginous with thin, purple, violet, yellow sandy siltstone with streaks of gypseous clay, carbonaceous bands and rare plant remains
Jaisalmer		Jajiya	Oxfordian	Yellow oolitic, bioturbated, cross-stratified limestone and sandstone
	Kuldhar		Callovian	Fossiliferous oolitic silty marl, shell beds, shales and limestones
	BadaBag		Mid-Upper Bathonian	Marly mudstone, siltstone, sandstone, well-cemented shelly and arenaceous limestones with hardgrounds
	Fort		Lower Bathonian–Bajocian	Poorly to moderately cemented sandstones, fossiliferous bioturbated to cross-stratified limestones
	Joyan			Trough cross-stratified limestones with erosional surfaces and reworked large coral heads, bioturbated limestones and fine-grain sandstone
	Hamira			Cross-stratified calcareous sandstone
Lathi	Thaiat		Bajocian–Lower Jurassic	White to grey, poorly cemented, fine-grained, often calcareous sandstone, multi-coloured sandy siltstone and a red siltstone bed
	Odania			Pebbly unit followed by a white to maroon, sandy siltstone, coarse dark ferruginous sandstone, arkosic, coarse, poorly sorted sandstone

3 Sampling and methods

The most notable outcrops of the Kuldhar Member, which were investigated, are situated approximately 16 kms southwest of Jaisalmer. Two specific sections, namely, the Kuldhar River and Kuldhar Nala sections, were measured for this study. A total of fifteen representative limestone samples were collected from these sections, with coordinates recorded as N 26°51′55″ and E 70°44′07″ for the Kuldhar River Section and N 26°52′2.8″ and E 70°46′56.6″ for the Kuldhar Nala Section. A petrographical study of the limestone is carried out to identify the textural and compositional constituents, as well as diagenetic processes modifying these limestones. This study is carried out using a polarizing microscope (Laborlux 11 Pol 8) at the Department of Geology, Aligarh Muslim University, Aligarh. Fifteen representative samples were selected for geochemical analysis. These samples were pulverized using a jaw crusher and a TEMA mill equipped with an agate disc to obtain finely powdered material for the geochemical investigations. Subsequently, 6 g of the powdered samples were used to produce pellets for X-ray Fluorescence (XRF) analysis, employing the pressed pellet method. The major oxides present in the samples were determined using the Bruker S8 TIGER RF spectroscopy instrument at the Wadia Institute of Himalayan Geology (WIHG), Dehradun. In addition, to determine the Loss on Ignition (LOI), 5 g of sample powders were heated in a muffle furnace at approximately 1000 °C for 4 h. It is worth noting that the Bruker S8 TIGER instrument provides an analytical precision of around ± 5% to ± 6% for the major oxide measurements.

Rare Earth Elements (REEs) concentration analysis was carried out using an Inductively Coupled Plasma Mass Spectrometer (ICP-MS) instrument, specifically the Perkin Elmer SCIEX ELAN RDC-e at the Wadia Institute of Himalayan Geology (WIHG), Dehradun. For this analysis, approximately 0.1 g of sample powder was digested in a solution consisting of a 1:3 ratio of $HF + HNO_3$. Subsequently, 2 millilitres of $HClO_4$ were added to Teflon crucibles during the digestion process. The samples were digested using an open system method, where they were heated on a hot plate until a suitable precipitate consistency was achieved. Twenty millilitres of 10% HNO_3 were added to the precipitate, followed by another round of heating to bring the solution to the boiling point, resulting in a clear solution. Subsequently, the solution was allowed to cool, and milli-Q water was added to bring it to a final volume of 100 millilitres. It is important to note that the error percentage for REEs typically falls between 1% and 8%, while the instrument's accuracy ranges

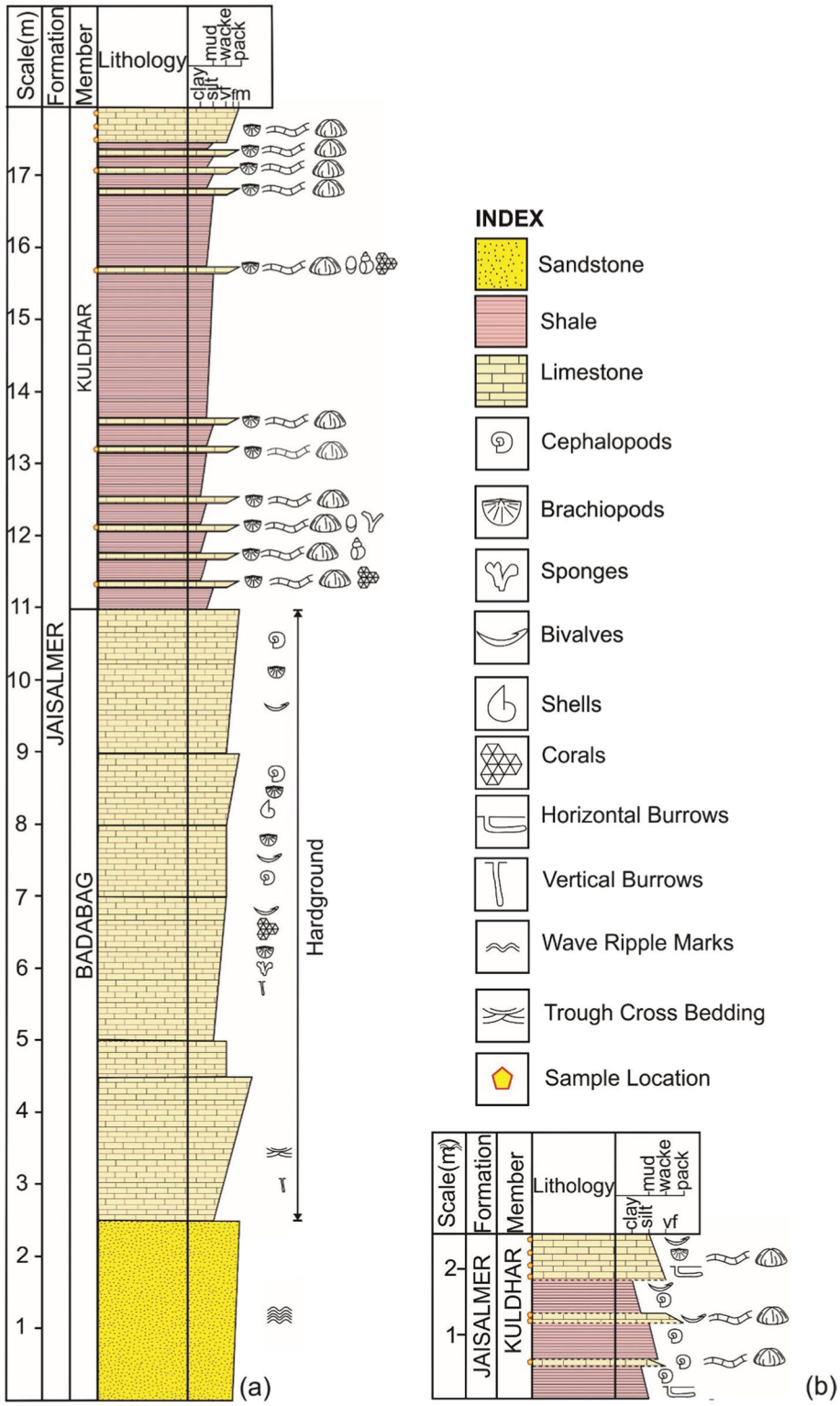

Fig. 2 Lithostratigraphic columns showing various lithologies of the Kuldhar Member succession of the Jaisalmer Formation. **a** Kuldhar River Section; **b** Kuldhar Nala Section

from 2% to 12%. To calibrate the analytical run, a range of international standards (such as SDO1, SGR1, GXR2, GXR6, SO1, GSS11, GSS4, and GSS9) were utilized. The REE normalized diagrams were prepared using the PAAS normalized values provided by Taylor and McLennan (1985).

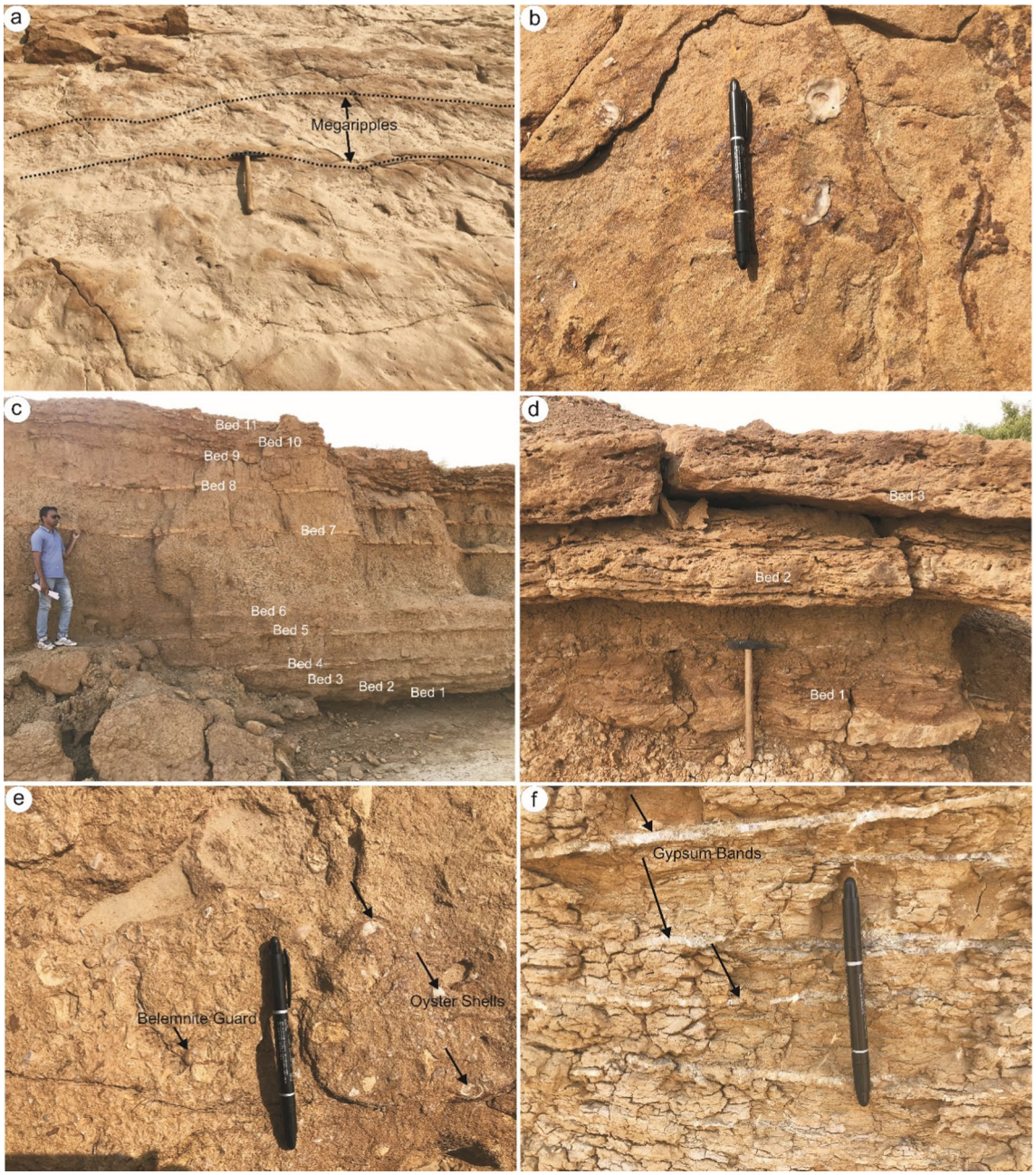

Fig. 3 Field photographs showing **a** Mega ripples formed on the limestone of Badabag Member exposed east of the dry beds of Kuldhar River (Length of hammer 33 cm); **b** Hardground containing oyster shell at the base of Kuldhar River Section (length of pen—12 cm); **c** complete Kuldhar River Section exposed around the dry beds of Kuldhar River south of ruined Kuldhar village showing poorly cemented alternate beds of limestone and shale (Height of person 5′11″); **d** complete Kuldhar Nala Section showing more compact and well-cemented beds of limestone and shale (Length of hammer 33 cm); **e** top most bed of Kuldhar Nala Section showing abundant fossil shells (length of pen—12 cm); **f** zoomed view of the gypsum bands precipitated in the shales (length of pen—12 cm)

4 Results

4.1 Petrography

The limestone samples are thoroughly examined under the microscope to analyse their constituent components, including skeletal and non-skeletal grains, cement, textural characteristics, and diagenetic features. The petrographical observations indicate that the KML is dominated by skeletal grains, which include brachiopods (Fig. 4a), corals (Fig. 4a), algae (Fig. 4a), foraminifera (Fig. 4b), bivalves (Fig. 4c), echinoderms (Fig. 4b, d), and ostracods

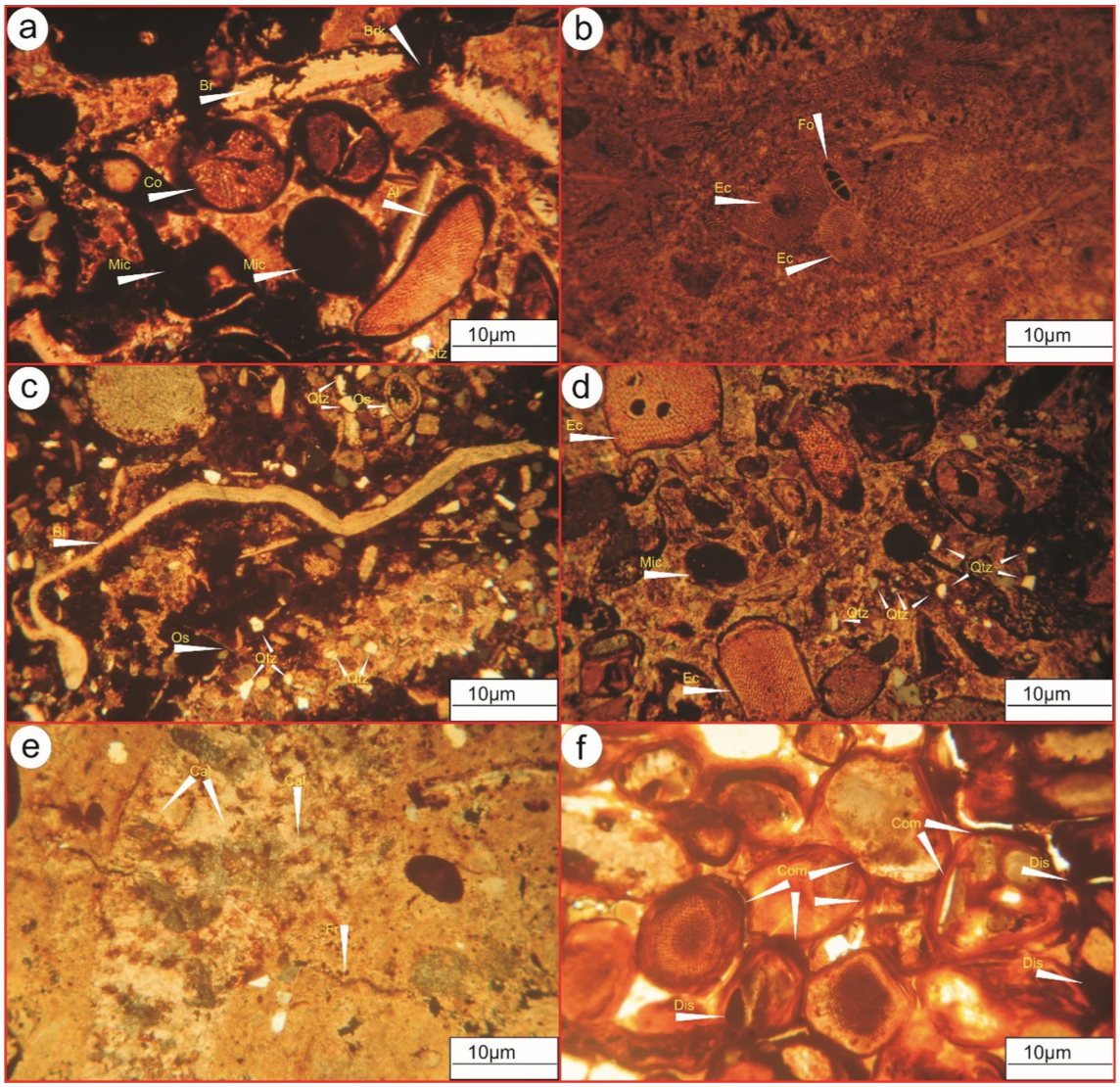

Fig. 4 Photomicrographs showing observed skeletal and non-skeletal components along with diagenetic features **a** Brachiopod, algae, coral along with presence of quartz admixture, micritization and mechanical compaction which lead to breaking of the brachiopod; **b** echinoderm and foraminifera fossils; **c** presence of bivalve, ostracods along with scattered quartz grains as terrigenous admixture; **d** echinoderm, quartz admixture and micritization; **e** presence of fracture and calcite cement; **f** compaction and dissolution as seen in KML

(Fig. 4c). Terrigenous input is exclusively dominated by quartz admixture (Fig. 4a, c, d). The KML is subjected to early marine, meteoric and burial diagenesis, as indicated by micritization (Fig. 4a, d), cementation (Fig. 4e), fracturing (Fig. 4e), physical and chemical compaction (Fig. 4f) which led to breaking (Fig. 4a) and dissolution (Fig. 4f) of the allochems.

4.2 Major oxides

The distribution of major oxides in limestones is largely determined by the proximity of the basin to continents, topographic elevation, and tectonic settings. The concentration of major oxide in Kuldhar Member Limestone is presented in Table 2. The significant abundance of CaO as a major oxide in the KML indicates that the precipitation of $CaCO_3$ predominantly occurred from seawater. The concentration of Fe_2O_3 is slightly higher, ranging from 3.72% to 29.09%, with an average of 9.73 wt% (Table 2). The silica concentration in these samples ranges from 1.25 wt% to 14.56 wt%, with an average of 5% (Table 2), while Al_2O_3 concentration varies from 0.29 wt% to 7.53 wt%, with an average of 1.76 wt% (Table 2). All of these samples exhibit a high LOI, ranging from 23.26 wt% to 42.07 wt%, and it shows a strong positive correlation with CaO (r = 0.99) (Table 3). Other significant oxides, such as TiO_2, K_2O, Na_2O, and P_2O_5, have concentrations ranging from 0.02–0.22%, 0.04–0.45%, 0.03–1.16%, and 0.02–1.33%

Table 2 Chemical concentration of some major oxides and strontium (wt%) for Kuldhar Member Limestone, Jaisalmer Formation, western Rajasthan

Sample Id	KL1	KL2	KL3	KL4	KL5	KL6	KL7	KL8	K3L1	K3L2	K3L3	K3L4	K3L5	K3L6	K3L1A
SiO_2	14.56	3.62	5.05	7.67	2.35	5.80	6.28	7.54	1.25	6.98	2.03	2.26	3.29	3.35	2.99
Al_2O_3	7.53	0.63	1.96	2.85	0.49	1.51	2.18	2.83	0.29	2.27	0.55	0.65	1.05	1.06	0.62
Fe_2O_3	29.09	6.73	15.91	15.61	3.72	6.36	6.76	10.46	5.04	8.18	6.12	5.80	9.94	9.43	6.75
CaO	19.78	47.74	38.46	35.47	50.76	43.95	43.57	39.32	49.93	41.83	48.58	48.74	44.52	44.24	46.89
MgO	2.54	0.65	1.21	1.35	0.40	0.90	1.06	2.24	1.18	1.50	1.16	0.91	1.31	1.67	1.71
K_2O	0.45	0.09	0.30	0.45	0.11	0.18	0.23	0.24	0.04	0.20	0.07	0.10	0.10	0.11	0.08
Na_2O	1.16	0.07	0.26	0.45	0.04	0.30	0.24	0.18	0.03	0.13	0.03	0.03	0.08	0.06	0.04
MnO	0.08	0.13	0.17	0.16	0.11	0.07	0.09	0.08	0.11	0.08	0.09	0.08	0.09	0.09	0.09
TiO_2	0.22	0.05	0.11	0.18	0.05	0.07	0.10	0.12	0.02	0.10	0.04	0.05	0.05	0.06	0.04
P_2O_5	1.33	0.04	0.51	0.15	0.02	0.06	0.14	0.11	0.05	0.85	0.04	0.02	0.39	0.20	0.02
L.O.I	23.26	40.25	36.06	35.68	41.95	40.80	39.36	36.87	42.07	37.88	41.30	41.35	39.17	39.73	40.75
Sum + L.O.I	100.00	100.00	100.00	100.00	100.00	100.00	100.00	100.00	100.00	100.00	100.00	100.00	100.00	100.00	100.00
Sr	0.030	0.009	0.001	0.001	0.010	0.020	0.015	0.015	0.013	0.021	0.015	0.022	0.017	0.013	0.013

(Table 2). Low percentages of TiO_2, Al_2O_3, Na_2O, and K_2O, are observed and show positive correlation with SiO_2 (Table 3). All the other major oxides exhibit positive correlations with each other, except for CaO and, in some cases, MnO (Table 3).

4.3 Rare earth elements

The rare earth elements (REEs) form a cohesive group of elements that exhibit similar ionic radii and trivalent oxidation states under most physico-chemical conditions in the Earth's crust (Bau, 1991). In the KML, the total content of REEs varies between 0.64 and 449.88 mg kg^{-1}, with an average concentration of 155.50 mg kg^{-1} (Table 4). The concentrations of light rare earth elements (LREE) in these samples range from 0.51 to 381.79 mg kg^{-1}, while heavy rare earth elements (HREE) concentrations range from 0.13 to 68.09 mg kg^{-1}. ∑REE exhibits a weakly positive correlation with Al_2O_3 (r = 0.03), and SiO_2 (0.1) and a weakly negative correlation with CaO (r = -0.08). The Post-Archean Australian Shale (PAAS) normalized REE pattern of typical seawater demonstrate a depletion of LREE, a negative Ce anomaly, and a slight positive La anomaly (Baar, 1991; Bau & Dulski, 1996). In contrast, non-seawater REE patterns are often LREE-enriched, with a positive Gd anomaly and a negative Ce anomaly. The REE pattern of KML is normalised with PAAS, showing non-seawater-like properties with a nearly flat pattern (Fig. 5). The majority of the samples have positive Ce and Gd anomalies, whereas all of them have positive Eu anomalies. The average $(Nd/Yb)_{SN}$ ratio is 1.20, while the $(La/Yb)_{SN}$ ratio ranges from 0.43 to 1.33, with an average of 0.84. The $(Dy/Yb)_{SN}$ ratio ranges from 0.61 to 2.44 with an average of 1.42 (Table 4).

5 Discussion

The predominance of CaO over MgO implies that calcite was the primary mineral phase in these carbonates, with minimal to no dolomite present. Since dolomite is rarely observed in petrographic investigations, it is reasonable to conclude that the concentrations of MgO in the samples are unrelated to dolomite. This conclusion is further supported by the Mg v Ca plot (Fig. 6), which clearly shows that the analysed samples fall well below the stoichiometric dolomite line given by Johnson et al. (2010). Moreover, the strong negative correlation observed between CaO and MgO (r = − 0.77) suggests that the fractionation of these elements did not occur simultaneously. This indicates that MgO might be present in minor silicate phases within the rocks or incorporated into the structural lattice of calcite. Ca is primarily biogenic origin (Fig. 4a-–e), and regardless of its initial distribution, it serves as a dilutant for all other major oxides, as well as for ∑REE, as indicated by its negative correlation with all other components. The high LOI values and its strong positive correlation with CaO (r = 0.99) indicates that CaO is primarily supplied from carbonate sources, with LOI in calcite rather than plagioclase. Focusing on Fe, the strong correlation between Fe_2O_3 and Al_2O_3 (r = 0.93) (Table 3) suggests a robust relationship between Fe and the aluminosilicate component. This excess Fe is most likely the component adsorbed on clays, explaining both the high correlation between Fe_2O_3 and Al_2O_3 as well as the excess Fe (Murray et al., 1992). The positive correlation of TiO_2, Al_2O_3, Na_2O, and K_2O, with SiO_2, indicates that these

Table 3 Correlation coefficient matrix for Kuldhar Member Limestone, Jaisalmer Formation, western Rajasthan

	SiO_2	Al_2O_3	Fe_2O_3	CaO	MgO	K_2O	Na_2O	MnO	TiO_2	P_2O_5	L.O.I	La	Ce	Pr	Nd	Sm	Eu	Gd	Tb	Dy	Ho	Er	Tm	Yb	Lu	∑REE
SiO_2	1.00																									
Al_2O_3	**0.98**	1.00																								
Fe_2O_3	**0.89**	**0.93**	1.00																							
CaO	**− 0.96**	**− 0.97**	**− 0.98**	1.00																						
MgO	**0.70**	**0.74**	**0.75**	**− 0.77**	1.00																					
K_2O	**0.87**	**0.84**	**0.85**	**− 0.89**	0.50	1.00																				
Na_2O	**0.95**	**0.98**	**0.94**	**− 0.97**	0.70	**0.85**	1.00																			
MnO	**− 0.03**	**− 0.09**	0.13	**− 0.06**	**− 0.31**	**0.38**	0.00	1.00																		
TiO_2	**0.95**	**0.93**	**0.90**	**− − 0.95**	0.61	**0.98**	0.93	0.22	1.00																	
P_2O_5	**0.85**	**0.86**	**0.81**	**− 0.85**	0.73	**0.63**	0.79	− 0.20	**0.73**	1.00																
L.O.I	**− 0.95**	− 0.98	− 0.97	**0.99**	− 0.76	− 0.83	− 0.98	0.01	− 0.91	− 0.87	1.00															
La	− 0.02	− 0.09	− 0.10	0.04	0.08	0.03	− 0.22	0.00	− 0.01	0.27	0.11	1.00														
Ce	0.07	0.00	0.01	− 0.06	0.14	0.12	− 0.14	0.04	0.08	0.36	0.01	0.99	1.00													
Pr	0.14	0.07	0.04	− 0.11	0.20	0.12	− 0.08	− 0.08	0.10	0.45	− 0.05	0.97	0.99	1.00												
Nd	0.17	0.10	0.06	− 0.14	0.22	0.13	− 0.05	− 0.09	0.13	0.48	− 0.09	0.96	0.98	1.00	1.00											
Sm	0.19	0.11	0.07	− 0.15	0.23	0.14	− 0.04	− 0.11	0.14	0.49	− 0.10	0.94	0.97	0.99	1.00	1.00										
Eu	0.19	0.11	0.06	− 0.14	0.23	0.13	− 0.05	− 0.12	0.13	0.49	− 0.09	0.94	0.96	0.99	1.00	1.00	1.00									
Gd	0.18	0.10	0.07	− 0.14	0.22	0.14	− 0.05	− 0.09	0.13	0.48	− 0.09	0.95	0.97	0.99	1.00	1.00	1.00	1.00								
Tb	0.17	0.09	0.05	− 0.13	0.22	0.12	− 0.06	− 0.10	0.12	0.47	− 0.08	0.94	0.97	0.99	0.99	1.00	1.00	1.00	1.00							
Dy	0.15	0.07	0.04	− 0.11	0.20	0.11	− 0.08	− 0.09	0.10	0.45	− 0.06	0.95	0.97	0.99	0.99	1.00	1.00	1.00	1.00	1.00						
Ho	0.14	0.06	0.03	− 0.11	0.19	0.11	− 0.09	− 0.08	0.10	0.44	− 0.05	0.95	0.98	0.99	0.99	1.00	1.00	1.00	1.00	1.00	1.00					
Er	0.12	0.04	0.02	− 0.09	0.17	0.10	− 0.11	− 0.06	0.08	0.42	− 0.02	0.96	0.98	0.99	0.99	0.99	0.99	1.00	1.00	1.00	1.00	1.00				
Tm	0.12	0.05	0.03	− 0.10	0.19	0.12	− 0.11	− 0.06	0.09	0.42	− 0.03	0.96	0.98	0.99	0.99	0.99	0.99	0.99	0.99	0.99	1.00	1.00	1.00			
Yb	0.09	0.00	− 0.01	− 0.06	0.14	0.10	− 0.14	− 0.02	0.07	0.37	0.01	0.97	0.98	0.98	0.98	0.98	0.98	0.99	0.99	0.99	0.99	1.00	1.00	1.00		
Lu	0.10	0.03	0.02	− 0.09	0.17	0.11	− 0.12	− 0.04	0.08	0.39	− 0.02	0.96	0.98	0.98	0.98	0.98	0.98	0.98	0.98	0.99	0.99	0.99	1.00	1.00	1.00	
∑REE	**0.10**	**0.03**	0.02	**− 0.08**	0.17	0.11	− 0.11	− 0.03	**0.09**	**0.41**	− 0.02	0.98	1.00	1.00	0.99	0.99	0.98	0.99	0.99	0.99	0.99	0.99	0.99	0.99	0.99	1.00

Bold highlighted values are the significant correlations between various major and rare earth elements

Table 4 Rare earth element concentrations (mg kg^{-1}) for Kuldhar Member Limestone, Jaisalmer Formation, western Rajasthan

Sample Id	KL1	KL2	KL3	KL4	KL5	KL7	K3L1	K3L2	K3L3	K3L4	K3L5	K3L6	K3L1A	Average
La	8.55	0.12	36.55	25.23	26.44	20.13	18.01	60.81	16.84	16.93	39.26	27.40	23.80	24.62
Ce	27.19	0.23	102.70	69.18	60.54	45.56	40.04	170.22	34.11	37.18	107.95	72.82	52.99	63.13
Pr	4.69	0.04	11.33	7.22	6.83	5.93	4.79	23.24	3.95	4.29	13.52	8.80	6.12	7.75
Nd	20.98	0.09	45.72	28.65	26.03	23.25	18.21	98.84	14.54	15.96	56.62	35.82	22.89	31.35
Sm	4.41	0.02	9.94	6.08	4.50	5.32	3.51	23.25	2.94	3.10	12.86	7.63	4.46	6.77
Eu	1.00	0.01	2.30	1.37	0.96	1.35	0.82	5.44	0.66	0.77	3.00	1.77	0.99	1.57
Gd	4.18	0.02	10.44	6.27	4.37	5.16	3.61	23.44	2.96	3.27	13.27	7.77	4.30	6.85
Tb	0.60	0.01	1.59	0.92	0.59	0.84	0.53	3.66	0.44	0.55	2.08	1.19	0.67	1.05
Dy	2.70	0.02	8.50	4.98	3.11	4.58	2.81	18.97	2.40	2.59	11.17	6.11	3.61	5.50
Ho	0.51	0.01	1.70	0.99	0.61	0.89	0.55	3.65	0.48	0.59	2.13	1.23	0.73	1.08
Er	1.11	0.02	4.33	2.51	1.65	2.35	1.44	8.89	1.25	1.41	5.37	3.03	1.90	2.71
Tm	0.18	0.01	0.65	0.38	0.23	0.36	0.20	1.24	0.19	0.28	0.77	0.48	0.28	0.40
Yb	0.71	0.02	3.84	2.39	1.47	2.24	1.26	7.24	1.10	1.29	4.61	2.67	1.76	2.35
Lu	0.15	0.01	0.57	0.33	0.22	0.33	0.17	0.99	0.17	0.26	0.64	0.43	0.25	0.35
∑ LREE	66.81	0.51	208.53	137.72	125.30	101.55	85.37	381.79	73.04	78.22	233.21	154.24	111.25	135.19
∑ HREE	10.13	0.13	31.62	18.77	12.25	16.74	10.56	68.09	8.98	10.25	40.03	22.90	13.50	20.30
∑ REE	76.94	0.64	240.15	156.49	137.54	118.29	95.93	449.88	82.02	88.47	273.24	177.15	124.74	155.50
Ce/Ce*	0.99	0.74	1.16	1.18	1.04	0.96	0.99	1.04	0.96	1.00	1.08	1.08	1.01	1.02
Eu/Eu*	1.08	2.40	1.05	1.03	1.01	1.20	1.07	1.09	1.05	1.13	1.07	1.07	1.05	1.18
Pr/Pr*	1.12	1.57	0.94	0.92	0.98	1.04	1.01	1.02	1.01	1.00	0.98	0.98	1.00	1.04
Gd/Gd*	1.06	0.34	1.07	1.10	1.14	0.95	1.07	1.03	1.07	0.98	1.04	1.05	1.04	0.99
$(Nd/Yb)_N$	2.60	0.39	1.04	1.05	1.55	0.91	1.27	1.19	1.16	1.08	1.07	1.17	1.14	1.20
$(Dy/Yb)_N$	2.44	0.61	1.41	1.33	1.34	1.30	1.42	1.67	1.39	1.27	1.54	1.46	1.30	1.42
$(La/Yb)_N$	0.89	0.43	0.70	0.78	1.33	0.66	1.06	0.62	1.13	0.96	0.63	0.76	1.00	0.84
$(La/Nd)_N$	0.34	1.11	0.67	0.74	0.86	0.73	0.83	0.52	0.98	0.89	0.58	0.64	0.88	0.75
Er/Nd	0.05	0.20	0.09	0.09	0.06	0.10	0.08	0.09	0.09	0.09	0.09	0.08	0.08	0.09

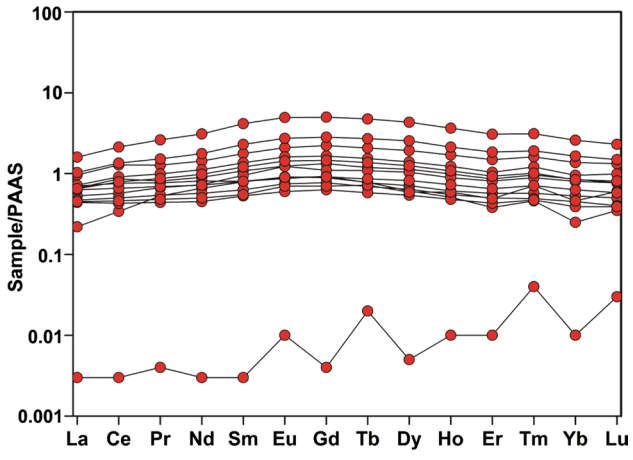

Fig. 5 PAAS normalized REE pattern of Kuldhar Member Limestone (KML), Jaisalmer Formation

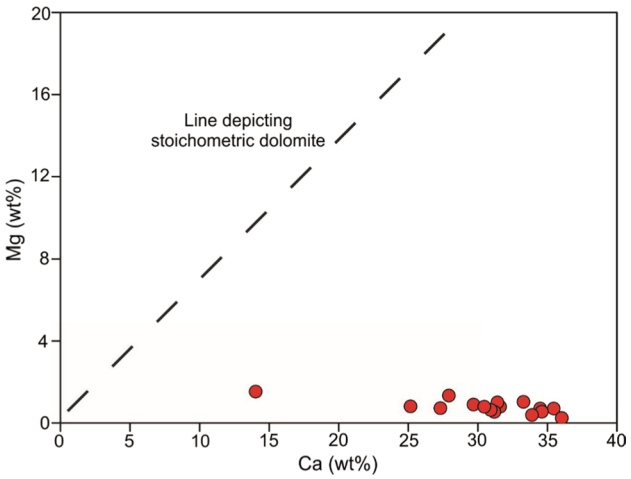

Fig. 6 Comparison of the Calcium and Magnesium content of Kuldhar Member Limestone (KML) of Jaisalmer Formation. Samples showing domination of Ca over Mg

elements are associated with the detrital influx, introduced as impurities to these carbonates (Fig. 4a, c, d) (Table 3) (Madhavaraju et al., 2017). This is further supported by the strong negative correlation between CaO and SiO_2 (Table 3).

5.1 Possible sources for REE in Kuldhar Member Limestone

The mobilization and differentiation of rare earth elements (REEs) occur when primary phases undergo weathering or alteration. This leads to the formation of secondary phases, where the weathering residue tends to display an enrichment of light rare earth elements (LREEs), while the weathering products exhibit an enrichment of heavy rare earth elements (HREEs) (Nesbitt, 1979). Various processes influence the enrichment and depletion of REEs in limestone, including: i) the input of REEs from the land through erosion and sedimentation (McLennan, 1989; Piper, 1974), ii) the deposition of REEs through biological processes from the overlying seawater (Murphy & Dymond, 1984; Nagarajan et al., 2011), iii) scavenging processes influenced by salinity and oxygen levels (Bertram & Elderfield, 1993; Elderfield, 1988; Piepgras & Jacobsen, 1992), and iv) the removal of REEs from the water column and early diagenesis through authigenic processes (Sholkovitz, 1988).

Shales have a higher REE concentration than carbonates, it may be assumed that terrigenous material with a non-seawater REE pattern contain significantly more REEs than marine carbonate phases (Nothdurft et al., 2004; Piper, 1974). The substantial increase in the concentration of REEs in carbonates can be attributed to the contamination of non-carbonate minerals such as silicates, Fe–Mn oxides, phosphates, or sulphides during chemical leaching (Zhao et al., 2009). REEs are key tracers in numerous geological and oceanic processes, making them essential for understanding these processes and their fractionation (Murray & Leinen, 1993; Piper, 1974). Negative Ce anomalies are common in carbonate minerals that precipitate in equilibrium with seawater, and they are observable in the REE patterns of limestones (Palmer, 1985).

The total rare earth element ($\sum$REE) content in pure carbonates is typically low. Therefore, an increase in their proportion is believed to result of contamination by oxides, sulphides, phosphates, or silicates, which could originate from magmatic–hydrothermal events or terrestrial particulate matter (Frimmel, 2009). In the case of the KML, the $\sum$REE concentration ranges from 0.64 mg kg^{-1} to 449.88 mg kg^{-1}, with an average of 155.50 mg kg^{-1} (Fig. 7; Table 4). The variation in $\sum$REE content among different samples is primarily due to differences in the extent of contamination by detrital influx. Except for sample KL-2, which has a $\sum$REE value of 0.64, all other samples display significantly higher $\sum$REE values compared to the range of marine carbonates (0.04–14 mg kg^{-1}; Turekian & Wedepohl, 1961) and the average for typical marine carbonates (~ 28 mg kg^{-1}; Bellanca et al., 1997).

The shale-normalized rare earth element (REE) pattern of the KML displays a relatively flat pattern with a slight enrichment in heavy rare earth elements (HREE), which differs somewhat from the ideal seawater-like pattern (Fig. 5). Non-seawater-like patterns in carbonates typically result from the mixing of terrestrial materials (Elderfield et al., 1990), the presence of iron and manganese oxides (Bau & Dulski, 1996), and phosphates (Byrne & Sholkovitz, 1996). Phosphates have a disproportionate affinity for incorporating REEs, and their alteration during diagenesis can further influence the REE distribution (Reynard et al., 1999). The $\sum$REE values reveal slight positive correlations with SiO_2, Al_2O_3, TiO_2 and Fe_2O_3, indicating that the detrital siliciclastic fraction plays a role in controlling the REEs, and moderately negative correlations with CaO, confirming CaO dilution (Table 3). P_2O_5 contents are strongly correlated with TiO_2 ($r = 0.73$), Fe_2O_3 ($r = 0.81$) and K_2O ($r = 0.63$) (Table 3), suggesting that some, or perhaps most, of the P_2O_5 contents in KML may not be biogenic origin. This is because TiO_2 and K_2O are primarily derived from aluminosilicate clastics, and Fe_2O_3 originates from hydrothermal Fe–Mn-oxyhydroxides (e.g., Murray, 1994). The observed $(Nd/Yb)_{SN}$ ratio in the KML (average 1.20) is considerably higher than the values typically found in modern shallow seawater (ranging from ~ 0.205 to 0.497 for 50 m water depth; Zhang & Nozaki, 1996). This indicates that these limestones have not retained their original seawater characteristics. These data indicate that the major LREE scavenging processes control the changes in the $(Nd/Yb)_{SN}$ ratio in limestones (Wyndham et al., 2004). The somewhat higher $(Nd/Yb)_{SN}$ ratio is owing to adsorption and/or scavenging, in which the LREEs are mostly adsorbed onto particle surfaces and retained in HREE solutions with smaller ionic radii. The $(La/Yb)_{SN}$ ratio, which indicates the relative behavior of light rare earth elements (LREEs) to heavy rare earth elements (HREEs), ranges from 0.43 to 1.33, with an average of 0.84 in the studied samples (Table 3). While some samples exhibit higher values, the average $(La/Yb)_{SN}$ value for the KML is lower than the values proposed by Condie (1991) [$(La/Yb)_{SN} = 1$] and Sholkovitz (1990) [$(La/Yb)_{SN} = 1.33$] for terrigenous particulate matter. The fluctuation in this ratio indicates variations in the amount of terrigenous material incorporated in different samples and the influence of LREE-depleted carbonate components, leading to an overall depletion of LREEs in these limestones. The average $(La/Yb)_{SN}$ ratio of KML is in accordance with Arabian Sea carbonate sediments (Nath et al., 1997; Table 5) and lower than both shallow marine carbonate sediments (Madhavaraju & Ramasamy, 1999) and Indian Ocean carbonate sediments (Nath et al., 1992). The $(Dy/Yb)_{SN}$ ratio in the KML ranges

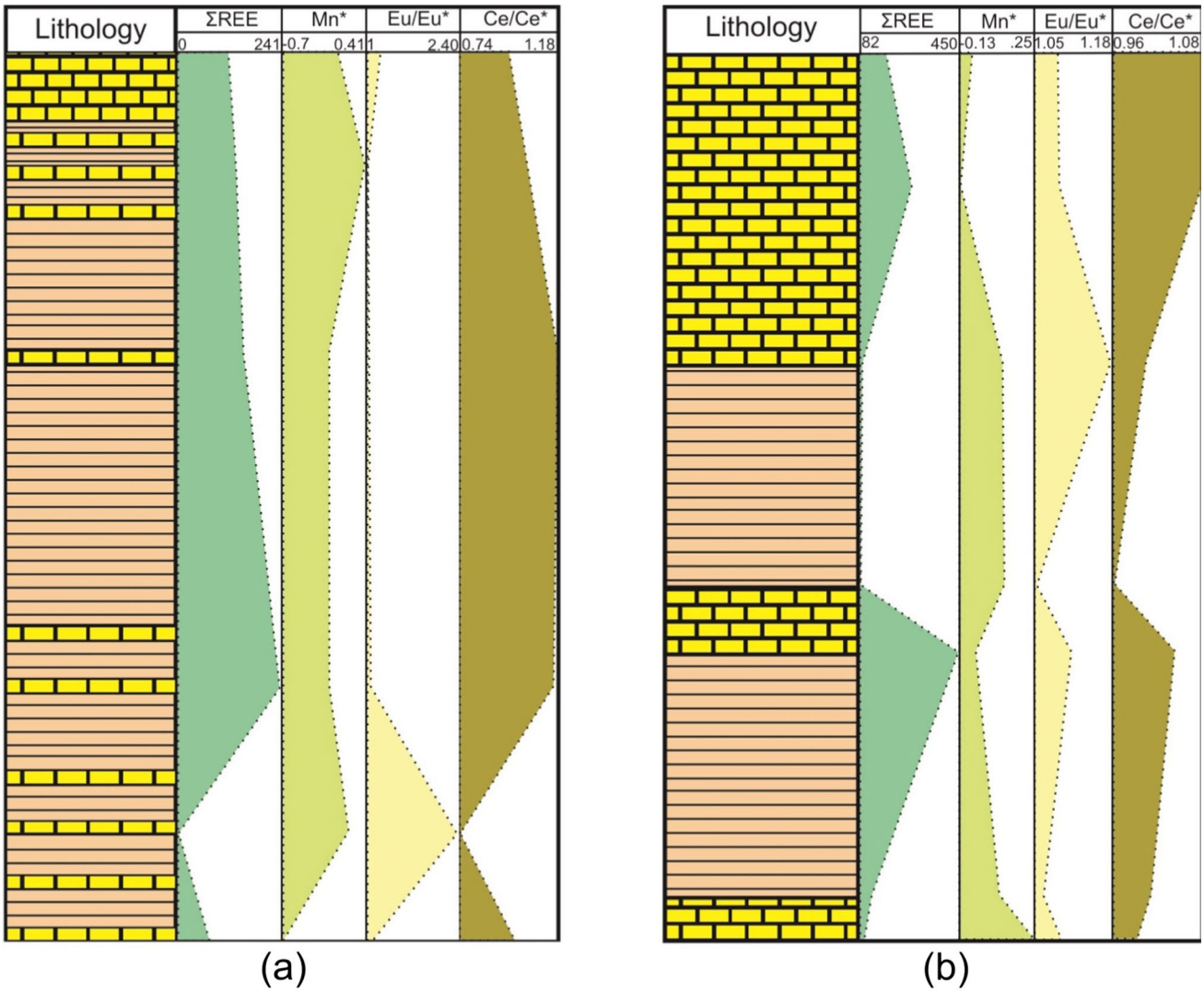

Fig. 7 Vertical variation of geochemical parameters indicating depositional environment and detrital influx **a** Kuldhar River Section **b** Kuldhar Nala Section

Table 5 Average values of Kuldhar Member Limestone (KML) compared to values of shallow, deep marine and Indian Ocean carbonate

	Kuldhar Member Limestone[a]	Shallow-marine carbonate[b]	Arabian sea carbonate[c]	Indian ocean carbonate[d]
Ce/Ce*	1.02	0.76 ± 0.16	0.84 ± 0.06	0.56
$(La/Yb)_N$	0.84	1.8 ± 0.5	0.8 ± 0.2	1.03
∑REE	155.5	73 ± 20	78 ± 40	–
$CaCO_3$	76.83	75 ± 15	51 ± 22	65.3
Eu/Eu*	1.18	0.58 ± 0.11	1.15 ± 0.08	–

[a]This study; $n = 15$

[b]Madhavaraju & Ramasamy, 1999; $n = 8$

[c]Nath et al., 1997; $n = 9$

[d]Nath et al., 1992

from 0.39 to 2.44, with an average of 1.42 (Table 4). This is similar to the $(Dy/Yb)_{SN}$ ratio found in shallow-marine carbonate (1.25 ± 0.23) (Madhavaraju & Ramasamy, 1999) and Indian Ocean carbonate (1.37 ± 0.05) (Nath et al., 1992) (Table 5). The high $(Dy/Yb)_{SN}$ ratio suggests an enrichment of HREEs rather than LREEs in the KML, similar to what is observed in modern seawater.

The Er/Nd ratio is used to interpret LREE/HREE fractionation effects in modern and ancient marine systems (German & Elderfield, 1989). In normal seawater, the Er/Nd ratio is around 0.27 (De Baar et al., 1988). The higher Er/Nd ratio in limestone indicates that the marine carbonates retained seawater signatures without significant contamination. However, the addition of detrital material or diagenetic alteration can reduce the Er/Nd values to less than 0.1 due to the preferential concentration of Nd compared to Er (Bellanca et al., 1997; De Baar et al., 1988). The Er/Nd ratio of the KML ranges from 0.05 to 0.2, with an average of 0.09 (Table 4), which is similar to that of shallow-marine carbonate.

The positive Eu anomaly observed in the KML (ranging from 1.05 to 2.40, average 1.18; Table 4) is attributed to the differentiation of Eu^{3+} ions from neighbouring elements as they are reduced to Eu^{2+}. The reduction of Eu^{3+} to Eu^{2+} reduces the radius of Eu ions, enabling their substitution for Ca^{2+} ions in the carbonate crystal lattice. The average Eu anomaly of KML is similar to Arabian Sea carbonate sediments (Nath et al., 1997; Table 5), and greater than shallow marine carbonate sediment (Madhavaraju & Ramasamy, 1999; Table 5), and Indian Ocean carbonate sediment (Nath et al., 1992; Table 5). In marine carbonate rocks, the positive Eu anomaly can be caused by the mixing of dust, river water, or hydrothermal fluids with seawater at mid-ocean ridges (Kamber & Webb, 2001; Nozaki et al., 1997), intense diagenesis (Murray et al., 1991a) or due to variation in plagioclase content (Nath et al., 1992). Since hydrothermal solutions mainly originate in the deep marine environment and KML is deposited in shallow marine depositional settings; it is highly unlikely that the hydrothermal solution affected the Eu concentration in KML. Another possible cause of the positive Eu anomaly in bulk sediments is a slight increase in the detrital feldspar component (Madhavaraju et al., 2010; Murray et al., 1991a). The elemental ratios K/Al and Na/Al are effective indicators of the presence of detrital feldspars in bulk sediments (Madhavaraju & Lee, 2009). However, in the present study, the K/Al and Na/Al ratios show almost no correlation with Eu/Eu* ($r = 0.07$ and 0.13, $n = 13$), indicating a minimal input of detrital feldspars in these limestones and ruling out their significant impact on the Eu anomaly.

A petrographical study of the KML indicates that the limestones were subjected to moderate to intense diagenesis, which is well-documented in the form of micritization (Fig. 4a, d), cementation and fracturing (Fig. 4e), mechanical compaction resulting in breaking of the allochem (Fig. 4a) and chemical compaction leading to dissolution (Fig. 4f) among others. Diagenesis, coupled with the input of terrigenous materials as indicated by petrographical studies (Fig. 4a, c, d) and higher REE concentrations, is likely responsible for the positive Eu anomaly.

5.2 Cerium anomaly and palaeo-redox conditions

Ce differs from other rare earth elements (REE) in its ability to undergo oxidation from Ce^{3+} to the less soluble Ce^{4+} state in saltwater, a characteristic not observed in other REE (Elderfield, 1988). This oxidation process allows Ce to precipitate in well-oxygenated seawater and become incorporated into marine sediments, resulting in a relative enrichment of Ce compared to other REE in those sediments (Bellanca et al., 1997). Scientists have utilized the Ce/Ce* ratio in sedimentary rocks to infer the conditions of seawater during the deposition of REE in marine sediments (German & Elderfield, 1990; Madhavaraju & Lee, 2009). The Ce/Ce* values observed in the KML range from 0.74 to 1.18 (Table 4), whereas the Ce/Ce* value in oceanic water is typically between 0.1 and 0.4 (Elderfield & Greaves, 1982), and shale exhibits a value of 1 (Murray et al., 1991b). A negative Ce anomaly is interpreted as an indication of oxidizing conditions during deposition, since Ce^{3+} is oxidized to Ce^{4+} under such conditions. Some samples may show a negative or positive Ce anomaly due to the enrichment of Ce relative to other REEs, caused by mobilization of Ce as Ce^{3+} under reducing conditions during early diagenesis and

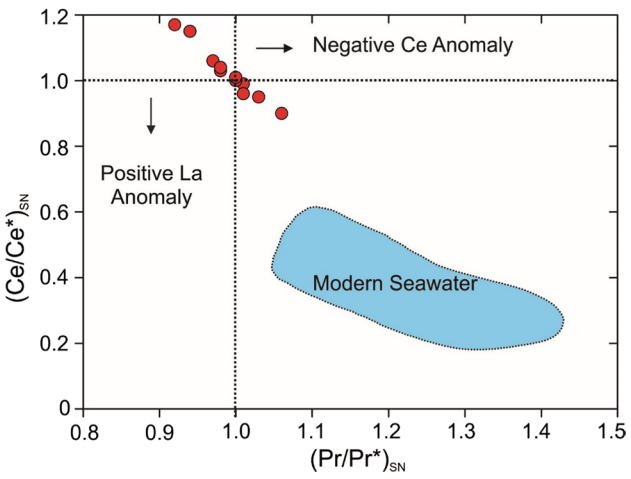

Fig. 8 Plot of Ce anomaly versus Pr anomaly for Kuldhar Member Limestone (Bau & Dulski, 1996). Range of modern seawater after Nagarajan et al (2011)

subsequent re-precipitation at the oxidized front (Mazumdar et al., 2003). The oxidizing conditions responsible for a positive Mn* value could also lead to the most negative Ce anomalies, while more reducing conditions, resulting in negative Mn* values, may produce the most positive Ce anomaly. Higher Ce/Ce* values in samples may indicate a greater contribution of terrigenous input, and vice versa. The Ce/Ce* values in these samples predominantly display positive anomalies with some negative anomalies (Fig. 8), confirming varying degrees of terrigenous input and indicating a fluctuating environment that alternated between oxic and anoxic conditions. The fluctuating Ce anomalies can also be explained using the bivariate diagram of Pr/Pr* versus Ce/Ce*, as proposed by Bau and Dulski (1996). The KML is plotted on the discriminant diagram (Fig. 8), falling within both the Ce negative anomaly field and the Ce positive anomaly field, further supporting the assertion of fluctuating depositional environmental conditions and varying degrees of detrital influx.

Manganese is extremely sensitive to reducing environmental conditions. A low redox potential (Eh) is usually favourable for the formation of a reduced, soluble form (Mn^{2+}) that then migrates to an oxic zone, where it undergoes re-oxidation and precipitation (Balzer, 1982; Calvert & Price, 1972). Sediments deposited in pelagic to hemipelagic environments undergo a transition from anoxic to oxic conditions, in which Mn enrichment begins in the pore waters of the reducing layer, and dissolved Mn may precipitate in the solid phase just below or above the redox boundary as it migrates upward (Bellanca et al., 1996). In KML, MnO concentrations exhibit little variation (0.08–0.16; average 0.1). These minor changes in MnO content could be attributed to variations in environmental conditions.

Reduced Fe and Mn are fractionated across the redox boundary due to their differing solubility potentials, with Fe being accommodated in sulphide under low Eh conditions and Mn being found in more oxygenated conditions above the redox boundary (Bellanca et al., 1996). To determine the redox potential of the depositional environment, Machhour et al. (1994) and Bellanca et al. (1996) presented the relationship $Mn^* = \log[(Mn_{sample}/Mn_{shales})/(Fe_{sample}/Fe_{shales})]$. For Mn_{shale} and Fe_{shale}, the mean values are 600 mg kg^{-1} and 46.150 mg kg^{-1}, respectively (Wedepohl, 1978). Mn* values in KML exhibit fluctuation, ranging from -0.64 to 0.41, with an average of -0.02 (Fig. 7). Positive Mn* values indicate oxic conditions, whereas negative Mn* values indicate a reducing deposition environment.

Based on all these values, it can be inferred that the depositional environment of KML experienced fluctuations between oxic and anoxic conditions. This fact is supported by the presence of both positive and negative 'Ce' anomalies as well as positive and negative Mn* values. However, since positive 'Ce' anomalies and negative Mn* value is dominant, it can be concluded that the environment was drastically reduced at the time of KML deposition.

The rocks in the Kuldhar Member of the Jaisalmer Formation were deposited in a fluctuating depositional environment, as indicated by the alternate shale and limestone beds in the Kuldhar Member (Fig. 3c). Limestones were deposited in a shallow marine environment, whereas the shales were deposited in a calmer and quitter deep marine environment. This changing depositional setting is attributed to the frequent events of sea level fluctuations during the Middle Jurassic as studied in detail by Hallam (1978, 2001). The short-term variations in sea level during Middle Jurassic were triggered by temperature variations on a global level, which may have also played a role in the changing oxic and anoxic environment of deposition for KML. Therefore, we can conclude that the deposition of KML was largely in accordance with the prevailing climatic conditions of the Middle Jurassic.

6 Conclusions

The following conclusions have been drawn from the detailed geochemical analysis of the KML:

- The KML of the Jaisalmer Formation of western Rajasthan dominantly contains CaO followed by Fe_2O_3 and SiO_2. CaO shows a strongly negative correlation with SiO_2 and Al_2O_3, suggesting that it likely produced as calcite mineral due to chemical and biochemical precipitation of seawater. SiO_2 and Al_2O_3 were introduced from siliciclastic sediments as terrigenous admixture. The presence of terrigenous admixture in these limestones is further supported by the negative correlation between ∑REE and CaO, along with a positive correlation with SiO_2, Al_2O_3 and TiO_2.
- The higher concentration of Fe_2O_3 is attributed to the component adsorbed on clays, and a strong relationship between Fe and the aluminosilicate component is also justified by the strong positive correlation observed between Fe_2O_3 and Al_2O_3.
- The PAAS normalized REE patterns of these limestones show a non-seawater-like pattern with flat LREE and a slight enrichment in HREE. The fluctuating Ce anomaly suggests varying depositional environment and varying degrees of detrital influx in these carbonates.
- The changing depositional environment is further confirmed by the presence of both positive and negative Mn* values, indicating fluctuations between oxic and anoxic conditions during deposition. The positive Eu anomaly in these limestones is due to terrigenous input, possibly resulting from continental weathering prod-

ucts transported into seawater. The low Er/Nd ratios suggest that these carbonates did not preserve their seawater characteristics, which is also confirmed by their high ∑REE concentration.

- The fluctuation in the depositional environment could be attributed to rapid changes in global climatic conditions during Middle Jurassic, resulting in the deposition of KML in a fluctuating oxic–anoxic environment.

Acknowledgements Authors are thankful to Chairperson, Department of Geology, Aligarh Muslim University, Aligarh for providing necessary facilities in the Department. Shaikh Asjad is grateful to the University Grants Commission (UGC), New Delhi, for the financial assistance in the form of Senior Research Fellowship (SRF). We would like to express our gratitude to the two anonymous reviewers for their critical comments and recommendations, which have significantly improved the quality of this manuscript. We thank Prof. Maria Virgínia Alves Martins, Editor-in-Chief, Journal of Sedimentary Environments for efficient editorial handling.

Author contributions SA: Carried out fieldwork, conception and design of the study, data analysis, drafting of the original manuscript. KFK: review and editing of manuscript and overall supervision. MAQ: Carried out fieldwork,Conception and design of the study, data analysis, drafting of the original manuscript, review and editing. AJ: Carried out fieldwork, and co-designed the work and contributed in the finalisation of manuscript

Funding The financial aid for the current work has been provided by the University Grants Commission (UGC), New Delhi, in the form of Senior Research Fellowship (SRF).

Availability of data and materials All the data generated or analysed during the present study are included in this manuscript.

Declarations

Conflict of interests The authors declare that they have no conflict of interests.

References

Ahmad, F., Amir, M., Quasim, M. A., Absar, N., & Ahmad, A. H. M. (2022). Petrography and geochemistry of the Middle Jurassic Fort Member Sandstone, Jaisalmer Formation, Western India: Implications for weathering, provenance, and tectonic setting. *Geological Journal, 57*(5), 1741–1758. https://doi.org/10.1002/gj.4372

Ahmad, F., Quasim, M. A., & Ahmad, A. H. M. (2020). Lithofacies characteristics and depositional environment interpretations of the middle Jurassic fort member rocks, Jaisalmer formation, Western Rajasthan, India. *Journal of Sedimentary Environments, 5*, 355–373. https://doi.org/10.1007/s43217-020-00023-6

Ahmad, F., Quasim, M. A., & Ahmad, A. H. M. (2021b). Microfacies and diagenetic overprints in the limestones of Middle Jurassic Fort Member (Jaisalmer Formation), Western Rajasthan, India: Implications for the depositional environment, cyclicity, and reservoir quality. *Geological Journal, 56*(1), 130–151. https://doi.org/10.1002/gj.3945

Ahmad, F., Quasim, M. A., Ahmad, A. H. M., Rehman, S. M., & Asjad, S. (2021a). Depositional mechanism of fort member sandstone (early-late bathonian), Jaisalmer formation, western Rajasthan: Insights from granulometric analysis. *Geology, Ecology, and Landscapes, 5*(2), 119–135. https://doi.org/10.1080/24749508.2020.1833642

Ahmad, F., Quasim, M. A., Ghaznavi, A. A., Khan, Z., & Ahmad, A. H. M. (2017). Depositional environment of the Fort Member of the Jurassic Jaisalmer Formation (western Rajasthan, India), as revealed from lithofacies and grain-size analysis. *Geologica Acta, 15*(3), 153–167. https://doi.org/10.1344/GeologicaActa2017.15.3.1

Asjad, S., Ahmad, A. H. M., Quasim, M. A., & Sachan, H. K. (2021). Provenance, palaeoweathering and tectonic setting of the Kuldhar Member Shale (Callovian–Oxfordian), Jaisalmer Formation, western Rajasthan. *Journal of Sedimentary Environments, 6*, 585–602. https://doi.org/10.1007/s43217-021-00072-5

Balzer, W. (1982). On the distribution of iron and manganese at the sediment/water interface: Thermodynamic versus kinetic control. *Geochimica Et Cosmochimica Acta, 46*, 1153–1161. https://doi.org/10.1016/0016-7037(82)90001-1

Banner, J. L., Hanson, G. N., & Meyers, W. J. (1988). Water-rock interaction history of regionally extensive dolomites of the Burlington-Keokuk Formation (Mississippian): isotopic evidence. In V. Shukla & P. Baker (Eds.), *Sedimentology and geochemistry of dolostones* (Vol. 43, pp. 97–113). Society of Economic Paleontologists and Mineralogists, Special Publication.

Bau, M. (1991). Rare-earth element mobility during hydrothermal and metamorphic fluid-rock interaction and the significance of the oxidation state of europium. *Chemical Geology, 93*, 219–230. https://doi.org/10.1016/0009-2541(91)90115-8

Bau, M., & Dulski, P. (1996). Distribution of yttrium and rare-earth elements in the Penge and Kuruman iron-formations, Transvaal supergroup, South Africa. *Precambrian Research, 79*, 37–55.

Bellanca, A., Claps, M., Erba, E., Masetti, D., Neri, R., Silva, I. P., & Venezia, F. (1996). Orbitally induced limestone/marlstone rhythms in the Albian—Cenomanian Cismon section (Venetian region, northern Italy): Sedimentology, calcareous and siliceous plankton distribution, elemental and isotope geochemistry. *Palaeogeography, Palaeoclimatology, Palaeoecology, 126*, 227–260. https://doi.org/10.1016/S0031-0182(96)00041-7

Bellanca, A., Masetti, D., & Neri, R. (1997). Rare earth elements in limestone/marlstone couplets from the Albian-Cenomanian Cismon section (Venetian region, northern Italy): assessing REE sensitivity to environmental changes. *Chemical Geology, 25*, 141–152. https://doi.org/10.1016/S0009-2541(97)00058-2

Bertram, C. J., & Elderfield, H. (1993). The geochemical balance of the rare earth elements and neodymium isotopes in the oceans. *Geochimica Et Cosmochimica Acta, 57*, 1957–1986. https://doi.org/10.1016/0016-7037(93)90087-D

Byrne, R. H., & Sholkovitz, E. R. (1996). Marine chemistry and geochemistry of the lanthanides. In K. A. Gschneider Jr. & L. Eyring (Eds.), *Handbook on the Physics and Chemistry of the Rare Earths* (Vol. 23, pp. 497–593). Elsevier, Amsterdam. doi:https://doi.org/10.1016/S0168-1273(96)23009-0

Calvert, S. E., & Price, N. B. (1972). Diffusion and reaction profiles of dissolved manganese in the pore waters of marine sediments. *Earth and Planetary Science Letters, 16*, 245–249. https://doi.org/10.1016/0012-821x(72)90197-5

Condie, K. C. (1991). Another look at rare earth elements in shales. *Geochimica Et Cosmochimica Acta, 55*, 2527–2531. https://doi.org/10.1016/0016-7037(91)90370-K

Das Gupta, S. K. (1975). A revision of the Mesozoic-Tertiary stratigraphy of the Jaisalmer Basin, Rajasthan. *Indian Journal of Earth Science, 2*, 77–94.

De Baar, H. J. (1991). On cerium anomalies in the Sargasso Sea. *Geochimica Et Cosmochimica Acta, 55*, 2981–2983. https://doi.org/10.1016/0016-7037(91)90463-F

De Baar, H. J. W., German, C. R., Elderfield, H., & Van Gaans, P. (1988). Rare earth element distributions in anoxic waters of the Cariaco Trench. *Geochimica Et Cosmochimica Acta, 52*, 1203–1219. https://doi.org/10.1016/0016-7037(88)90275-X

Elderfield, H. (1988). The oceanic chemistry of the rare-earth elements. *Philosophical Transactions of the Royal Society a: Mathematical, Physical and Engineering Sciences, 325*, 105–126. https://doi.org/10.1098/rsta.1988.0046

Elderfield, H., & Greaves, M. J. (1982). The rare earth elements in seawater. *Nature, 296*, 214–219. https://doi.org/10.1038/296214a0

Elderfield, H., Upstill-Goddard, R., & Sholkovitz, E. R. (1990). The rare earth elements in rivers, estuaries, and coastal seas and their significance to the composition of ocean waters. *Geochimica Et Cosmochimica Acta, 54*, 971–991. https://doi.org/10.1016/0016-7037(90)90432-K

Frimmel, H. E. (2009). Trace element distribution in Neoproterozoic carbonates as palaeoenvironmental indicator. *Chemical Geology, 258*, 338–353. https://doi.org/10.1016/j.chemgeo.2008.10.033

Fu, X., Wang, J., Zeng, Y., Tan, F., & He, J. (2011). Geochemistry and origin of rare earth elements (REEs) in the Shengli River oil shale, northern Tibet, China. *Geochemistry, 71*, 21–30. https://doi.org/10.1016/j.chemer.2010.07.003

German, C. R., & Elderfield, H. (1989). Rare earth elements in Saanich Inlet, British Columbia, a seasonally anoxic basin. *Geochimica Et Cosmochimica Acta, 53*, 2561–2571. https://doi.org/10.1016/0016-7037(89)90128-2

German, C. R., & Elderfield, H. (1990). Application of the Ce anomaly as a paleoredox indicator: the ground rules. *Paleoceanography and Paleoclimatology, 5*, 823–833. https://doi.org/10.1029/PA005i005p00823

Hallam, A. (1978). Eustatic cycles in the Jurassic. *Palaeogeography, Palaeoclimatology, Palaeoecology, 23*, 1–32. https://doi.org/10.1016/0031-0182(78)90079-2

Hallam, A. (2001). A review of the broad pattern of Jurassic sea-level changes and their possible causes in the light of current knowledge. *Palaeogeography, Palaeoclimatology, Palaeoecology, 167*, 23–37. https://doi.org/10.1016/S0031-0182(00)00229-7

Jain, S. (2008). Integrated Jurassic biostratigraphy: a closer look at nannofossil and ammonite evidences from the Indian subcontinent. *Current Science, 95*, 326–331.

Johnson, C. A., Taylor, C. D., Leventhal, J. S., & Freitag, K. (2010). Geochemistry of metasedimentary rocks in the hanging wall of the Greens Creek massive sulfide deposit and of shales elsewhere on Admiralty Island. In C. D. Taylor & C. A. Johnson (Eds.), *Geology, Geochemistry, and Genesis of the Greens Creek Massive Sulfide Deposit, Admiralty Island, Southeastern Alaska* (Vol.1763, pp. 159–82). US Geological Survey Professional Paper.

Kachhara, R. P., & Jodhawat, R. L. (1981). On the age of Jaisalmer Formation, Rajasthan, India. *Proceedings of IX Indian Colloquium on Micropalaeontology and Stratigraphy*, 235–247.

Kamber, B. S., & Webb, G. E. (2001). The geochemistry of late Archaean microbial carbonate: Implications for ocean chemistry and continental erosion history. *Geochimica Et Cosmochimica Acta, 65*, 2509–2525. https://doi.org/10.1016/S0016-7037(01)00613-5

Liu, Y. G., Miah, M. R., & Schmitt, R. A. (1988). Cerium: A chemical tracer for paleo-oceanic redox conditions. *Geochimica Et Cosmochimica Acta, 52*, 1361–1371.

Lv, D., Fan, W., Ejembi, J. I., Wu, D., Wang, D., Li, Z., Li, J., & Li, P. (2020). Depositional environments of limestones from the Taiyuan Formation in the North China Block interpreted from REE proxies. *Carbonates and Evaporites, 35*, 1–10. https://doi.org/10.1007/s13146-020-00580-x

Machhour, L., Philip, J., & Oudin, J. L. (1994). Formation of laminite deposits in anaerobic—dysaerobic marine environments. *Marine Geology, 117*, 287–302. https://doi.org/10.1016/0025-3227(94)90021-3

Madhavaraju, J., González-León, C. M., Lee, Y. I., Armstrong-Altrin, J. S., & Reyes-Campero, L. M. (2010). Geochemistry of the mural formation (Aptian-Albian) of the Bisbee group, Northern Sonora, Mexico. *Cretaceous Reseasrch, 31*, 400–414. https://doi.org/10.1016/j.cretres.2010.05.006

Madhavaraju, J., & Lee, Y. I. (2009). Geochemistry of the Dalmiapuram Formation of the Uttatur Group (Early Cretaceous), Cauvery basin, Southeastern India: Implications on provenance and paleo-redox conditions. *Revista Mexicana De Ciencias Geologicas, 26*, 380–394.

Madhavaraju, J., Löser, H., Scott, R. W., Sandeep, S., Sial, A. N., & Ramasamy, S. (2017). Petrography, geochemistry and stable isotopes of carbonate rocks, Lower Cretaceous Alisitos Formation, Los Torotes section, Baja California, Mexico. *Revista Mexicana De Ciencias Geologicas, 34*, 63–77. https://doi.org/10.22201/cgeo.20072902e.2017.2.45

Madhavaraju, J., & Ramasamy, S. (1999). Rare earth elements in limestones of Kallankurichchi Formation of Ariyalur Group, Tiruchirapalli Cretaceous, Tamil Nadu. *Journal of Geological Society of India, 54*, 291–301.

Mazumdar, A., Tanaka, K., Takahashi, T., & Kawabe, I. (2003). Characteristics of rare earth element abundances in shallow marine continental platform carbonates of Late Neoproterozoic successions from India. *Geochemical Journal, 37*, 277–289. https://doi.org/10.2343/geochemj.37.277

McLennan, S. M. (1989). Rare earth elements in sedimentary rocks: Influence of provenance and sedimentary processes. *Geochemistry and Mineralogy of Rare Earth Elements, 21*, 169–200. https://doi.org/10.1515/9781501509032-010

Muecke, G. K., Pride, C., & Sarkar, P. (1979). Rare earth element geochemistry of regional metamorphic rocks. *Physics and Chemistry of the Earth, 11*, 449–464. https://doi.org/10.1016/0079-1946(79)90043-0

Murphy, K., & Dymond, J. (1984). Rare earth element fluxes and geochemical budget in the eastern equatorial Pacific. *Nature, 307*, 444–447. https://doi.org/10.1038/307444a0

Murray, R. W. (1994). Chemical criteria to identify the depositional environment of chert: general principles and applications. *Sedimentary Geology, 90*, 213–232.

Murray, R. W., Brink, M. R., Brumsack, H. J., Gerlach, D. C., & Russ, G. P., III. (1991a). Rare earth elements in Japan Sea sediments and diagenetic behavior of Ce/Ce∗: Results from ODP Leg 127. *Geochimica Et Cosmochimica Acta, 55*, 2453–2466. https://doi.org/10.1016/0016-7037(91)90365-C

Murray, R. W., Brink, M. R., Gerlach, D. C., Russ, G. P., III., & Jones, D. L. (1992). Interoceanic variation in the rare earth, major, and trace element depositional chemistry of chert: perspectives gained from the DSDP and ODP record. *Geochimica Et Cosmochimica Acta, 56*, 1897–1913. https://doi.org/10.1016/0016-7037(92)90319-E

Murray, R. W., & Leinen, M. (1993). Chemical transport to the seafloor of the equatorial Pacific Ocean across a latitudinal transect at 135 W: Tracking sedimentary major, trace, and rare earth element fluxes at the Equator and the Intertropical Convergence Zone. *Geochimica Et Cosmochimica Acta, 57*, 4141–4163. https://doi.org/10.1016/0016-7037(93)90312-K

Murray, R. W., Ten Brink, M. R., Gerlach, D. C., Russ, G. P., III., & Jones, D. L. (1991b). Rare earth, major, and trace elements in chert from the Franciscan Complex and Monterey Group, California: assessing REE sources to fine-grained marine sediments. *Geochimica Et Cosmochimica Acta, 55*, 1875–1895. https://doi.org/10.1016/0016-7037(91)90365-C

Nagarajan, R., Madhavaraju, J., Armstrong-Altrin, J. S., & Nagendra, R. (2011). Geochemistry of Neoproterozoic limestones of

the Shahabad formation, Bhima basin, Karnataka, southern India. *Geosciences Journal, 15*, 9–25. https://doi.org/10.1007/s12303-011-0005-0

Narayanan, K., Subrahmanyan, M., & Srinivasan, S. (1961). *Geology of Jaisalmer*. Unpublished report ONGC Dehradun.

Nath, B. N., Bau, M., Rao, B. R., & Rao, C. M. (1997). Trace and rare earth elemental variation in Arabian Sea sediments through a transect across the oxygen minimum zone. *Geochimica Et Cosmochimica Acta, 61*, 2375–2388. https://doi.org/10.1016/S0016-7037(97)00094-X

Nath, B. N., Roelandts, I., Sudhakar, M., & Plüger, W. L. (1992). Rare earth element patterns of the Central Indian Basin sediments related to their lithology. *Geophysical Research Letters, 19*, 1197–1200. https://doi.org/10.1029/92GL01243

Nesbitt, H. W. (1979). Mobility and fractionation of rare earth elements during weathering of a granodiorite. *Nature, 279*, 206–210. https://doi.org/10.1038/279206a0

Nothdurft, L. D., Webb, G. E., & Kamber, B. S. (2004). Rare earth element geochemistry of Late Devonian reefal carbonates, Canning Basin, Western Australia: Confirmation of a seawater REE proxy in ancient limestones. *Geochimica Et Cosmochimica Acta, 68*, 263–283. https://doi.org/10.1016/S0016-7037(03)00422-8

Nozaki, Y., Zhang, J., & Amakawa, H. (1997). The fractionation between Y and Ho in the marine environment. *Earth and Planetary Science Letters, 148*, 329–340. https://doi.org/10.1016/S0012-821X(97)00034-4

Palmer, M. R. (1985). Rare earth elements in foraminifera tests. *Earth and Planetary Science Letters, 73*, 285–298. https://doi.org/10.1016/0012-821X(85)90077-9

Pandey, D. K., Fürsich, F. T., & Sha, J. (2009). Interbasinal marker intervals – A case study from the Jurassic basins of Kachchh and Jaisalmer, western India. *Sciences in China Series D: Earth Sciences, 52*, 1924–1931. https://doi.org/10.1007/s11430-009-0158-0

Pandey, D., & Pooniya, D. (2015). Sequence stratigraphy of the Oxfordian to Tithonian sediments (Baisakhi Formation) in the Jaisalmer Basin. *Volumina Jurassica, 13*, 65–76. https://doi.org/10.5604/17313708.1148658

Pandey, D. K., Sha, J., & Choudhary, S. (2010). Sedimentary cycles in the Callovian-Oxfordian of the Jaisalmer Basin, Rajasthan, western India. *Volumina Jurassica, 8*, 131–162.

Patra, A., & Singh, B. P. (2017). Geochemistry of the Eocene limestones of the Jaisalmer basin, Rajasthan, India: Implications on depositional conditions and sources of rare earth elements. *Geochemistry International, 55*, 1180–1192. https://doi.org/10.1134/S0016702917120023

Piepgras, D. J., & Jacobsen, S. B. (1992). The behavior of rare earth elements in seawater: Precise determination of variations in the North Pacific water column. *Geochimica Et Cosmochimica Acta, 56*, 1851–1862. https://doi.org/10.1016/0016-7037(95)00061-4

Piper, D. Z. (1974). Rare earth elements in the sedimentary cycle: A summary. *Chemical Geology, 14*, 285–304. https://doi.org/10.1016/0009-254(74)90066-7

Reineck, H. E., & Singh, I. B. (1980). *Tidal flats in Depositional sedimentary environments* (pp. 430–456). Berlin, Heidelberg: Springer. https://doi.org/10.1007/978-3-642-81498-3_26

Reynard, B., Lécuyer, C., & Grandjean, P. (1999). Crystal-chemical controls on rare-earth element concentrations in fossil biogenic apatites and implications for paleoenvironmental reconstructions. *Chemical Geology, 155*, 233–241. https://doi.org/10.1016/S0009-2541(98)00169-7

Sholkovitz, E. R. (1988). Rare earth elements in the sediments of the North Atlantic Ocean, Amazon Delta, and East China Sea; reinterpretation of terrigenous input patterns to the oceans. *American Journal of Science, 288*, 236–281. https://doi.org/10.2475/ajs.288.3.236

Sholkovitz, E. R. (1990). Rare-earth elements in marine sediments and geochemical standards. *Chemical Geology, 88*, 333–347. https://doi.org/10.1016/0009-2541(90)90097-Q

Singh, B. P., Srivastava, V. K., & Kanhaiya, S. (2019). Sedimentological and geochemical characteristics of the late middle Eocene dolostone succession, Kachchh, western India. *Geological Journal, 54*(6), 3840–3859. https://doi.org/10.1002/gj.3378

Srivastava, S. K. (1966). Jurassic microflora from Rajasthan, India. *Micropalaeontology, 12*, 87–103.

Swami Nath, J., Krishnamurthy, J. G., Verma, K. K., & Chandak, G. J. (1959). General geology of Jaisalmer area, Rajasthan. In ECAFE symposium on Mineral Research and Development p. 54–155

Taylor, S. R., & McLennan, S. M. (1985). *The continental crust: Its composition and evolution*. Blackwell Scientific Publishing.

Toyoda, K., Nakamura, Y., & Masuda, A. (1990). Rare earth elements of Pacific pelagic sediments. *Geochimica Et Cosmochimica Acta, 54*, 1093–1103. https://doi.org/10.1016/0016-7037(90)90441-M-

Turekian, K. K., & Wedepohl, K. H. (1961). Distribution of the elements in some major units of the earth's crust. *Geological Society of America Bulletin, 72*, 175–192. https://doi.org/10.1130/0016-7606(1961)72[175:DOTEIS]2.0.CO;2

Wan, Y., Wang, J., Fang, W., Fu, X., Wang, Z., & Shen, L. (2017). Characteristics and indications of rare earth elements in carbonates in the Buqu formation, southern Qiangtang Basin. *Petroleum Geology and Experiment, 39*, 655–665. https://doi.org/10.11781/sysydz201705655

Webb, G. E., & Kamber, B. S. (2000). Rare earth elements in Holocene reefal microbialites: a new shallow seawater proxy. *Geochimica Et Cosmochimica Acta, 64*, 1557–1565. https://doi.org/10.1016/S0016-7037(99)00400-7

Wedepohl, K. H. (1978). Manganese: abundance in common sediments and sedimentary rocks. Handbook of geochemistry (pp 1–17). Springer, Berlin.

Wyndham, T., McCulloch, M., Fallon, S., & Alibert, C. (2004). High-resolution coral records of rare earth elements in coastal seawater: Biogeochemical cycling and a new environmental proxy. *Geochimica Et Cosmochimica Acta, 68*, 2067–2080. https://doi.org/10.1016/j.gca.2003.11.004

Zhang, J., & Nozaki, Y. (1996). Rare earth elements and yttrium in seawater: ICP-MS determinations in the East Caroline, Coral Sea, and South Fiji basins of the western South Pacific Ocean. *Geochimica Et Cosmochimica Acta, 60*, 4631–4644. https://doi.org/10.1016/S0016-7037(96)00276-1

Zhao, Y. Y., Zheng, Y. F., & Chen, F. (2009). Trace element and strontium isotope constraints on sedimentary environment of Ediacaran carbonates in southern Anhui, South China. *Chemical Geology, 265*, 345–362. https://doi.org/10.1016/j.chemgeo.2009.04.015